Preventive effects of transcutaneous CO_2 application on disuse osteoporosis and muscle atrophy in a rat hindlimb suspension model

Nishida, Ryota ; Fukui, Tomoaki ; Niikura, Takahiro ; Kumabe, Yohei ; Yoshikawa, Ryo ; Takase, Kyohei ; Yamamoto, Yuya ; Kuroda, Ryosuke ;…

(Citation)
Bone,189:117262

(Issue Date)
2024-12

(Resource Type)
journal article

(Version)
Version of Record

Bone 189 (2024) 117262

Contents lists available at ScienceDirect

Bone

journal homepage: www.elsevier.com/locate/bone

Full Length Article

Preventive effects of transcutaneous CO_2 application on disuse osteoporosis and muscle atrophy in a rat hindlimb suspension model

Ryota Nishida [a], Tomoaki Fukui [a], Takahiro Niikura [b], Yohei Kumabe [a], Ryo Yoshikawa [a], Kyohei Takase [a], Yuya Yamamoto [a], Ryosuke Kuroda [a], Keisuke Oe [a,*]

[a] Department of Orthopaedic Surgery, Kobe University Graduate School of Medicine, Japan
[b] Department of Orthopaedic Surgery, Hyogo Prefectural Nishinomiya Hospital, Japan

ARTICLE INFO

Keywords:
Transcutaneous CO_2 application
Hindlimb suspension
Disuse osteoporosis
Muscle atrophy
Angiogenesis
PGC-1α

ABSTRACT

We previously demonstrated that transcutaneous CO_2 application promotes muscle fiber-type switching, fracture healing, and osteogenesis by increasing blood flow and angiogenesis. Here, we aimed to investigate the preventive effects of transcutaneous CO_2 application on disuse osteoporosis and muscle atrophy in a rat hindlimb suspension model. Eleven-week-old male Sprague-Dawley rats were divided into hindlimb suspension (HS), HS with transcutaneous CO_2 application ($HSCO_2$), and control groups. $HSCO_2$ rats were administered transcutaneous 100 % CO_2 gas in their bilateral hindlimbs, five times a week for 20 min. After 3 weeks, we harvested the gastrocnemius, femur, and tibia for assessment. Histological analysis revealed a significant decrease in the gastrocnemius myofiber cross-sectional area in HS rats compared to the control rats, whereas $HSCO_2$ rats exhibited a significant increase compared to HS rats. Micro-computed tomography showed significant bone atrophy in the trabecular and cortical bones of the femur in HS rats compared to those of the control rats, whereas significant improvement was noted in $HSCO_2$ rats. Histological analysis of the proximal tibia revealed more marrow adipose tissue in the HS rats than in the control rats. However, in the $HSCO_2$ rats, fewer marrow adipose tissue and osteoclasts were observed. Moreover, $HSCO_2$ rats had more osteoblasts and higher expression of peroxisome proliferator-activated receptor gamma coactivator 1-alpha (PGC-1α) and vascular endothelial growth factor (VEGF) than the HS rats. The gastrocnemius and distal femur of $HSCO_2$ rats also exhibited elevated PGC-1α and VEGF expression and upregulation of the myogenesis markers and osteogenesis markers compared to those of HS rats. This treatment effectively prevented disuse osteoporosis and muscle atrophy by promoting local angiogenesis and blood flow. PGC-1α is crucial for promoting this angiogenic pathway. Transcutaneous CO_2 application may be a novel preventive procedure for disuse osteoporosis and muscle atrophy, complementing medication and rehabilitation.

1. Introduction

The increasing prevalence of disuse osteoporosis and muscle atrophy presents a significant challenge in the aging society. Almost half of all women and one-quarter of men older than 50 years are predicted to sustain osteoporosis-related fractures [1]. As prolonged bed rest causes disuse osteoporosis and muscle atrophy [2], early surgery and rehabilitation are crucial to prevent exacerbation [3,4]. Disuse osteoporosis and muscle atrophy treatment include rehabilitation and medication; however, few options are available. We previously designed an easy, non-invasive, topical system for the transcutaneous application of CO_2 gas. Through in vivo studies, we demonstrated the favorable effect of this

Abbreviations: Av, all bone volume; AV/MV, adipocyte volume per total bone marrow volume; AV/N.A, volume of each adipocyte per number of adipocytes; Ct. Th, cortical thickness; Cv, cortical bone volume; HS, hindlimb suspension; $HSCO_2$, hindlimb suspension with transcutaneous CO_2; Mv, medullary volume; N.A/MV, number of adipocytes per unit area of marrow volume; PGC-1α, peroxisome proliferator-activated receptor gamma coactivator 1-alpha; PI3K, phosphoinositide 3-kinase; PPAR, peroxisome proliferator-activated receptor; RANK, receptor activator of nuclear factor kappa-β; RANKL, receptor activator of nuclear factor kappa-β ligand; ROI, region of interest; RT-PCR, reverse transcription polymerase chain reaction.

* Corresponding author at: Department of Orthopaedic Surgery, Kobe University Graduate School of Medicine, 7-5-1, Kusunoki-cho, Chuo-ku, Kobe 650-0017, Japan.

E-mail address: keisukeo@med.kobe-u.ac.jp (K. Oe).

https://doi.org/10.1016/j.bone.2024.117262
Received 26 July 2024; Received in revised form 17 September 2024; Accepted 17 September 2024
Available online 18 September 2024

treatment on bone, including accelerated fracture union [5], osteogenesis in bone defects [6], and the suppression of bone destruction caused by cancer metastasis [7]. In our previous studies on rats focusing on muscles, we found that this therapy induced muscle fiber-type switching, mitochondrial biogenesis [8], and inhibition of muscle atrophy following sciatic nerve crush and fracture [9,10].

These effects can be explained by the Bohr effect, which facilitates O_2 dissociation from hemoglobin and upregulates O_2 pressure in the local tissues, thereby promoting microcirculation and local blood flow [11]. This therapy activates vascular endothelial growth factor (VEGF) via peroxisome proliferators-activated receptor (PPAR)-gamma coactivator-1 (PGC-1α), showing biological responses like those induced by exercise [8]. The VEGF-mediated stimulation of angiogenesis and blood flow contributes to fracture healing and osteogenesis [5,6]. Given the close relationship between angiogenesis and osteogenesis [12], transcutaneous CO_2 application might be useful in osteoporosis treatment. However, its effects on disuse osteoporosis remain unclear.

We hypothesized that transcutaneous CO_2 application can prevent disuse osteoporosis and muscle atrophy by promoting angiogenesis. Therefore, we aimed to investigate this hypothesis using a rat hindlimb suspension model, a recognized rodent model for characterizing disuse bone and muscle atrophy and simulating spaceflight [13].

2. Materials and methods

2.1. Animals

Thirty-nine 11-week-old male Sprague-Dawley rats (SLC Japan, Shizuoka, Japan) with a mean weight (± SD) of 371.7 g (± 13.2 g) were used in this study. The experiments adhered to the ARRIVE guidelines and were approved by the Animal Care and Use Committee of the Kobe University Graduate School of Medicine (P220701). The rats were randomly divided into the hindlimb suspension (HS), hindlimb suspension with transcutaneous CO_2 ($HSCO_2$), and ground control groups. They were housed individually under a 12-h light/dark cycle and controlled temperature conditions (23.5–25.5 °C) and had free access to food and water. After 3 weeks, the rats were euthanized through intraperitoneal administration of pentobarbital sodium, and the gastrocnemius muscles, femurs, and tibias were harvested for analysis.

2.2. Hindlimb suspension model

The HS and $HSCO_2$ rats were suspended from the ceiling of the cages using a specialized clip for rat hindlimb suspension (Yamashita Technical Research Institute Co., Ltd., Tokushima, Japan) attached to their tails (Supplemental Fig. 1A, B). They were maintained in a 30° head-down tilt position to keep their hindlimbs off the ground, even when the animal was fully stretched, allowing 360° free movement for eating and drinking [14]. Tail suspension continued for 3 weeks. Rats with normal cage activity served as the ground control group.

2.3. Transcutaneous CO_2 application

Transcutaneous CO_2 was applied to both hindlimbs of the rats as previously described [5]. Briefly, after the $HSCO_2$ rats were taken out of hindlimb suspension and sedated with a minimum dose of isoflurane, both limbs were shaved, and a hydrogel (META MEDICINE LAB, Osaka, Japan), which enhances CO_2 absorption, was applied. The hydrogel (pH 5.5) comprised a carbomer, glycerin, sodium hydroxide, sodium alginate, sodium dihydrogen phosphate, methylparaben, and deionized water. Both hindlimbs were sealed in plastic bags filled with 100 % CO_2 for 20 min (Supplemental Fig. 1C). This treatment was performed 5 days a week for 3 weeks. To ensure consistency across groups, the rats in the control and HS groups were also anesthetized and underwent a sham treatment in which CO_2 was replaced with air. During the sham treatment, HS rats were also briefly removed from hindlimb suspension.

2.4. Bodyweight measurement

Body weight was measured at the beginning and end of the experiments and compared among all groups ($n = 13$ per group).

2.5. Wet muscle weight and histological analysis of the gastrocnemius

After 3 weeks, the rats were euthanized and the gastrocnemius muscles were dissected and harvested ($n = 7$ per group). The average weight of the bilateral wet muscles was measured, and the muscle-to-body weight ratio was calculated. The muscles were frozen and stored at −80 °C. The histological conditions for freezing the muscles were controlled at resting length when animals were sacrificed. Axial sections with a thickness of 9 mm were cut from the midpoint along the longitudinal axis using a cryostat, and hematoxylin and eosin (H&E) staining was performed. Muscle fibers were analyzed under 20× magnification using an optical microscope (BZ-X710, KEYENCE, Osaka, Japan), and the average myofiber cross-sectional area (CSA) was calculated in four randomly selected fields (1920 mm × 1440 mm/field) using ImageJ software (NIH, Bethesda, MD, USA).

2.6. Micro-quantitative computed tomography (μCT) analysis of the femur

Micro-CT was performed to assess the microarchitectural properties of the right femur (R_mCT2; RIGAKU, Tokyo, Japan) ($n = 7$ per group). For cortical bone evaluation, 1320-μm thick sections distal to the mid-shaft were used as the region of interest (ROI) [15]. Cortical bone parameters included all bone volume (Av), cortical bone volume (Cv), cortical bone ratio (Cv/Av), medullary volume (Mv), and cortical thickness (Ct.Th). For trabecular bone evaluation, the ROI was defined as the area located 2000 μm proximal to the epiphyseal plate to include the secondary trabecular spongiosa. Trabecular bone parameters included bone volume fraction (BV/TV), trabecular number (Tb.N), separation (Tb.Sp), and thickness (Tb.Th). All CT parameters were evaluated using TRI/3-D-BON software (Ratoc System Engineering, Tokyo, Japan).

2.7. Histological analysis of the proximal tibia

The right tibias were isolated, fixed in 4 % paraformaldehyde for 36 h, decalcified in 10 % ethylenediaminetetraacetic acid (EDTA) for 3 weeks, and embedded in paraffin. Coronal sections with a thickness of 6 μm were cut and stained with H&E, alkaline phosphatase (ALP), or tartrate-resistant acid phosphatase (TRAP). ALP and TRAP staining were performed using a staining kit (#294–67,001 FUJIFILM Wako) according to the manufacturer's instructions. For H&E staining, the histomorphometric parameters included adipocyte volume per total bone marrow volume (AV/MV, %), the number of adipocytes per unit area of marrow volume (N.A/MV, number of cells/mm^2), and the volume of each adipocyte per number of adipocytes (AV/N.A, μm^2). These parameters were measured in the bone marrow of the proximal tibia under 20× magnification using optical microscopy [16].

To evaluate osteoblast activity in the ALP-stained sections, the osteoblast number (Ob.N) along the trabecular bone surface were measured. The osteoblast surface (Ob.S) was evaluated as the length of the lining surface divided by the bone surface (BS) under 40× magnification. Osteoclast parameters (Oc. N/BS and Oc. S/BS) were analyzed in TRAP-stained sections under 20× magnification. TRAP-positive multinucleated cells containing more than three nuclei were counted as osteoclasts. In all sections, the ROI was the secondary spongiosa, including the metaphyseal area from 0.2 to 2.2 mm distal to the growth zone cartilage [17]. The average parameters of the bones were calculated from three randomly selected fields using ImageJ software ($n = 7$ per group).

2.8. Immunohistochemistry (IHC)

Paraffin-embedded right tibia sections were used for immunohistochemical assessment of the bone. After deparaffinization and hydration, the sections were treated with proteinase K (DAKO, CA, USA) and quenched with 0.05 % H_2O_2. Subsequently, the sections were incubated at 37 °C for 2 h in Can Get Signal Immunostain Solution A (Toyobo, Osaka, Japan) with the following primary antibodies: mouse anti-VEGF antibody (1:200; sc-7269, Santa Cruz, CA, USA) and mouse anti-peroxisome proliferator-activated receptor gamma coactivator 1-alpha (PGC-1α) antibody (1:200; sc-518,025, Santa Cruz, CA, USA). After washing, the sections were incubated with a horseradish peroxidase-conjugated anti-mouse antibody (1:200; 424,131, Histofine Simplestain Max PO; Nichirei, Tokyo, Japan) for an additional 30 min at room temperature. A brown reaction product, obtained using the peroxidase substrate 3,3-diaminobenzidine (Nichirei Bioscience, Tokyo, Japan), was considered the signal. Sections were counterstained with hematoxylin and examined under a microscope (BZ-X710). The ROI was determined as described in Section 2.7.

To investigate the effects of CO_2 therapy on the blood vessel density in the hindlimb muscles, we assessed capillary density in the gastrocnemius. Frozen sections of the right gastrocnemius were prepared in same manner as for H&E staining. Immunohistochemical staining of endothelial cells was performed using fluorescein-labeled isolectin B4 (Vector Laboratories, Burlingame, CA, USA). Nuclear staining was conducted with a 4′,6-diamidino-2-phenylindole solution (Nacalai Tesque, Kyoto, Japan) [5,10].

For both the bone and muscle samples, immunopositive areas were evaluated in three random fields under 20× magnification ($n = 7$ per group) using ImageJ software.

2.9. Gene expression assessment of the bones and muscles

The midsections of the right gastrocnemius and the right distal femur metaphysis were harvested and used to assess gene expression in the muscle and bone, respectively ($n = 6$ per group). For the bone samples, the entire bone, comprising both cortical and trabecular bone with accompanying marrow, was analyzed. Total RNA was extracted from tissues using a RNeasy Mini Kit (Qiagen, Valencia, CA, USA) and reverse transcribed into single-stranded DNA using a high-capacity cDNA reverse transcription kit (Applied Biosystems, Foster City, CA, USA). Real-time reverse transcription polymerase chain reaction (RT-PCR) was performed on cDNA in triplicate using an Applied Biosystems 7500 real-time RT-PCR system and SYBR Green reagent (Applied Biosystems). The expression level of each gene was normalized to that of glyceraldehyde-3-phosphate dehydrogenase (*GAPDH*), a housekeeping gene that served as an internal control. Results are presented as the fold-changes relative to the control group at 3 weeks, which were normalized to a value of 1 (ΔΔCt method). Gene expression data are shown in Supplemental Table 1.

2.10. Biomechanical assessment

Three weeks after suspension, the three-point bending strength of the left femoral diaphysis and the compression strength of the distal femoral metaphysis and femoral neck were measured (MZ-500S; Maruto Instrument Company, Tokyo, Japan). For the three-point bending test (Supplemental Fig. 2A), the femur was placed horizontally on a two-point sample holder (20 mm span) with the anterior aspect facing up. A 500 N load was applied on the center of the bone at a rate of 5.0 mm/min until the bone fractured.

After the femurs were separated into the distal and proximal parts during the three-point bending test, we proceeded with additional mechanical assessments. The distal half of the femur was used for the compression test (Supplemental Fig. 2B). In this test, the sample was placed on the test apparatus with the anterior aspect as the compression surface and compressed with a 500 N load at a rate of 5.0 mm/min until the maximum load was obtained or the compression distance was 3 mm. The proximal half of femur was used for the femoral neck compression test (Supplemental Fig. 2C). The sample was positioned facing upward in the test apparatus hole, with supported by the examiner's finger, and a 500 N load was applied to the femoral head from above at a rate of 5.0 mm/min.

For each test, the maximum load (N), stiffness (N/mm), breaking energy (N·mm), breaking force (N), and breaking time (s) were determined based on the load-displacement curve using the CTRwin software program, ver. 1.05 (System Supply Co., Ltd., Kanagawa, Japan) ($n = 7$ per group).

2.11. Statistical analysis

The normality of the data was verified using the Kolmogorov–Smirnov test. Differences between groups were evaluated using one-way analysis of variance (ANOVA) followed by the Tukey–Kramer post-hoc test. Data are presented as box and whisker plots, with median and interquartile ranges showing all data points. Outliers were defined as data points outside the whiskers of the box plot, with extreme values being at least 1.5 interquartile ranges below the first quartile or at least 1.5 interquartile ranges above the third quartile. All statistical analyses were performed using EZR (Saitama Medical Center, Jichi Medical University, Saitama, Japan), which is a graphical user interface for R (R Foundation for Statistical Computing, Vienna, Austria). Statistical significance was set at $p < 0.05$.

A post-hoc power analysis was performed using G*Power 3.1.9.7. Assuming a one-way ANOVA, for a sample size of seven samples in three groups and a type-I error (α) of 0.05, the study is expected to provide a power (1-β) of 0.81 for detecting an effect size of 0.75.

3. Results

3.1. Hindlimb suspension reduced rat body weight but transcutaneous CO_2 application did not

Body weights were comparable among all groups at the beginning of the experiment (Fig. 1A). After 3 weeks, the body weights of the HS and $HSCO_2$ rats were significantly lower than those of the control rats ($p < 0.0001$). However, no significant differences were observed between the HS and $HSCO_2$ groups (Fig. 1B). Therefore, hindlimb suspension caused reduced body weight but transcutaneous CO_2 application did not.

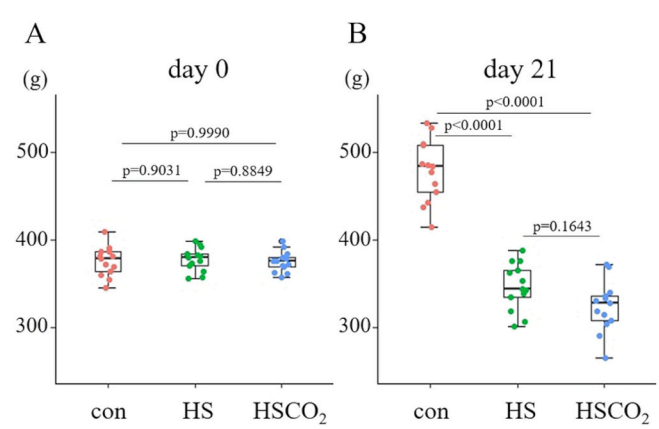

Fig. 1. The body weights on days 0 and 21 of the experiment. (A) Day 0. (B) Day 21. Data are presented as box plots with an indication of the median; whiskers represent the minimum to maximum values and indicate all points, $n = 13$. Outlier data points are indicated by black dots. Comparisons were performed using the one-way ANOVA followed by Tukey's test.

3.2. Transcutaneous CO_2 application suppressed the reduction of CSA induced by hindlimb suspension

Gastrocnemius wet muscle weight in HS rats was significantly lower than that in control rats ($p = 0.0025$). However, $HSCO_2$ rats showed no significant differences compared to the other groups (Fig. 2A). H&E staining showed that the average CSA of the gastrocnemius was significantly decreased in both HS and $HSCO_2$ rats than that in the control rats ($p < 0.0001$ and $p = 0.0019$, respectively). However, $HSCO_2$ rats had a significantly higher CSA than HS rats ($p = 0.0417$) (Fig. 2B, C).

3.3. Transcutaneous CO_2 application suppressed disuse osteoporosis induced by hindlimb suspension in both cortical and trabecular bones

Cortical bone analysis revealed that AV, CV, and Ct.Th levels were significantly lower in HS rats than in control rats ($p = 0.0013$, $p < 0.0001$, and $p = 0.0002$, respectively). Conversely, these parameters were significantly higher in $HSCO_2$ rats than those in HS rats ($p = 0.0342$, 0.0023, and 0.0233, respectively) but showed no significant difference from control rats. Cv/Av and Mv were not significantly different between the groups (Fig. 3B). Trabecular bone analysis indicated that all investigated parameters were significantly lower in HS rats than in control rats. $HSCO_2$ rats showed significantly higher BV/TV, Tb.N, and Tb.Sp values than HS rats ($p = 0.0342$, 0.0202, and 0.0113, respectively). These parameters in the $HSCO_2$ rats showed no significant differences from those in the control rats (Fig. 3C).

3.4. Transcutaneous CO_2 application suppressed the increase in marrow adipose tissue caused by hindlimb suspension and enhanced osteoblast activity while reducing osteoclast activity

AV/MV, AV/N.A and N. A/MV values were significantly higher in HS rats than in control rats ($p < 0.0001$, $p = 0.0031$, and $p < 0.0001$, respectively). In $HSCO_2$ rats, AV/MV was significantly lower than in HS rats ($p = 0.0499$). AV/N.A was lower in $HSCO_2$ rats than that in HS rats; however, the difference was not significant and the level was similar to that of the control rats. No significant difference was observed in N.A/MV between HS and $HSCO_2$ rats (Fig. 4A–C).

ALP staining showed that the Ob.N/BS and Ob.S/BS in HS rats were lower than those in control rats, but the differences were not significant. However, $HSCO_2$ rats showed significantly higher levels than HS rats ($p = 0.0344$ and 0.0024, respectively) (Fig. 4D, E). TRAP staining revealed similar Oc.N/BS and Oc.S/BS levels in control and HS rats, whereas those in $HSCO_2$ rats were significantly decreased compared to the other groups (Fig. 4F, G).

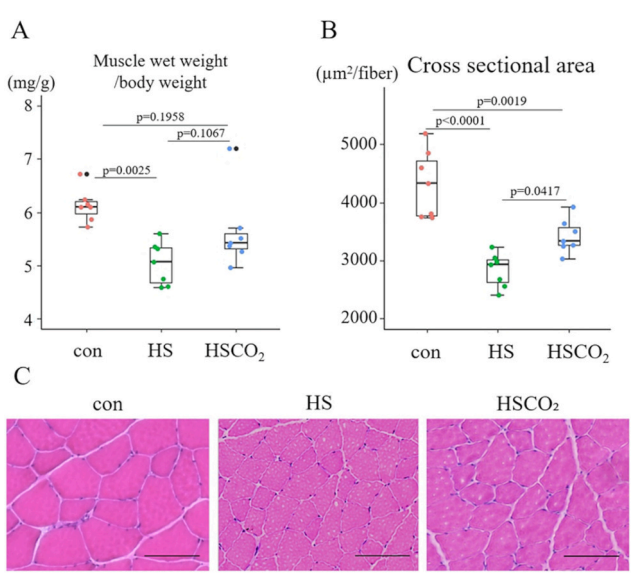

Fig. 2. The effect of transcutaneous CO_2 application on the gastrocnemius muscle. (A) Ratio of the wet gastrocnemius muscle weight to body weight at three weeks. (B) Quantitative analysis of the CSA per muscle fibers in gastrocnemius measured based on H&E staining images. (C) Representative H&E staining in gastrocnemius from the control, HS, and $HSCO_2$ rats. Scale bar, 100 μm. Data are presented as box plots with an indication of the median; whiskers represent minimum to maximum values and show all points, $n = 7$. Outlier data points are indicated with a black dot beside them. Comparisons were performed using the one-way ANOVA followed by Tukey's test.

3.5. Transcutaneous CO_2 application promoted VEGF and PGC-1α activity in the proximal tibia and increased capillary densities in the gastrocnemius

Sinusoids in the bone marrow, which are lined by endothelial cells, serve as a niche for hematopoietic stem cells, and their formation is crucial for establishing hematopoiesis [18]. Control rats exhibited a few adipocytes and many large sinusoids. VEGF-positive endothelial cells were observed within the sinusoid walls. In contrast, HS rats showed more adipocytes and fewer sinusoids VEGF- positive endothelial cells than the control rats. In the $HSCO_2$ rats, we observed more VEGF-positive endothelial cells and sinusoids than in the HS rats, suggesting increased angiogenesis in the $HSCO_2$ rats (Fig. 5A, B). Quantitative evaluation revealed that the number of positively stained areas for VEGF and PGC-1α in $HSCO_2$ rats was significantly higher than in the HS rats ($p = 0.0282$ and 0.0257, respectively). No significant difference was observed between the HS and control rats (Fig. 5D, E).

Visualization of capillaries in the gastrocnemius was performed using immunofluorescent isolectin B4 staining. In the $HSCO_2$ rats, more capillaries surrounding the muscle fibers were observed (Fig. 5F). Quantitative evaluation revealed that the isolectin B4-positive area was significantly larger in the $HSCO_2$ rats than in the control and HS rats ($p = 0.0086$ and 0.0002, respectively). No significant difference was found between the HS and control rats (Fig. 5G).

3.6. Transcutaneous CO_2 application upregulated myogenesis, osteogenesis, and angiogenesis markers in both muscle and bone

In the gastrocnemius, the expression of myoblast determination protein 1 (MyoD) was significantly higher in $HSCO_2$ rats than in HS rats ($p = 0.0341$). However, no significant differences in myogenin expression were observed among the groups. Among the muscle atrophic markers, Atrogin-1 expression was higher in the muscles of HS rats than in those of control rats ($p = 0.0155$). In the muscles of the $HSCO_2$ rats, the expression of Atrogin-1 and MuRF1 was significantly suppressed compared to those of the HS rats ($p < 0.0001$ and $p = 0.0269$, respectively). FOXO expression did not differ significantly among the groups. The expression of angiogenesis markers IGF-1 and eNOS in the muscles of the HS rats was lower than that in the control rats ($p = 0.0002$ and 0.0435, respectively). In the muscles of $HSCO_2$ rats, the expression of VEGF, PGC-1α, IGF-1, and eNOS were higher than that in HS rats ($p = 0.0012$, 0.0005, 0.0002, and 0.0471, respectively). The expression of HIF-1α in $HSCO_2$ rats was significantly suppressed compared to the controls ($p = 0.0371$), with no significant difference between HS and $HSCO_2$ groups (Fig. 6A).

The expression of osterix was lower in the bones of HS and $HSCO_2$ rats than that in those of the control group ($p = 0.0092$ and 0.0114, respectively), with no significant difference between HS and $HSCO_2$ rats. Although no significant differences were observed in Runx2 and ALP expression between the bones of control and HS rats, expression of these stains was significantly higher in the $HSCO_2$ rats ($p = 0.0214$ and 0.0065, respectively). Regarding angiogenesis markers, expression of VEGF and PGC-1α was significantly higher in $HSCO_2$ rats than that in HS rats ($p = 0.0178$ and 0.0149, respectively), and there were no significant differences in any other group comparisons. However, there was no

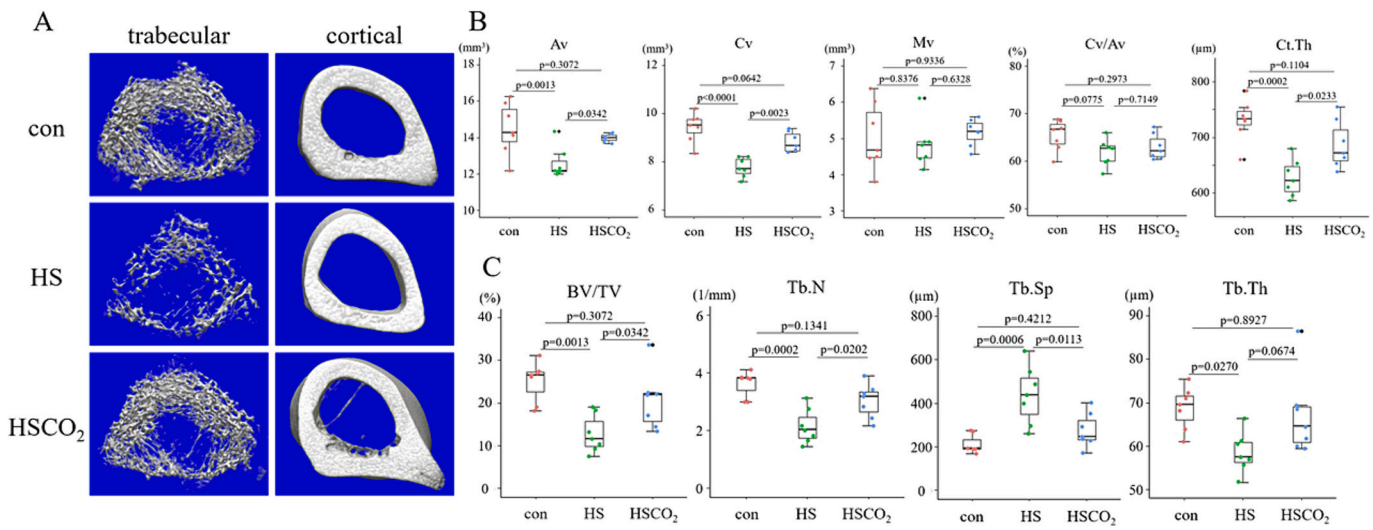

Fig. 3. Bone structural assessments evaluated with μCT. (A) Representative μCT images of cortical bones of midshaft femurs and trabecular bones of distal femurs isolated from the control, HS, and $HSCO_2$ rats. Cortical volume and trabecular density were reduced in HS rats than in control rats. The values were higher in $HSCO_2$ rats than in HS. (B) Quantitative μCT analysis of the cortical bone in the control, HS, and $HSCO_2$ rats. (C) Quantitative μCT analysis of the trabecular bone in the control, HS, and $HSCO_2$ rats. Data are presented as box plots with an indication of the median; whiskers represent minimum to maximum values and show all points, n = 7. Outlier data points are indicated with a black dot beside them. Comparisons were performed using one-way ANOVA followed by Tukey's test.

significant difference in the expression of HIF-1a among the groups. IL-6 expression was significantly increased in HS rats compared to that in control rats ($p = 0.0200$) and significantly decreased in $HSCO_2$ rats compared to HS rats ($p = 0.0311$) (Fig. 6B).

3.7. Transcutaneous CO_2 application suppressed the reduction in bone strength caused by hindlimb suspension in the distal femoral metaphysis and femoral neck

The biomechanical assessment revealed significant reductions in the breaking energy across all three tests in HS rats compared to the controls. However, no significant differences were observed between $HSCO_2$ and control rats. Significant reductions were observed in the maximum load of the distal femur compression test and in the breaking force of the femoral neck compression test in HS rats compared to controls. Conversely, significant increases were observed for these parameters for $HSCO_2$ rats compared to HS rats. Although the maximum load and stiffness in the femoral neck compression test did not differ significantly between HS and control rats, significant increases were observed in $HSCO_2$ rats compared to HS rats. The braking time was significantly lower in HS and $HSCO_2$ rats than in the control rats (Fig. 7A, B, C).

4. Discussion

Our findings suggest that transcutaneous CO_2 application does not affect the reduction in body weight caused by hindlimb suspension but prevents the reduction in muscle fiber CSA caused by hindlimb suspension. Moreover, it mitigates cortical and trabecular bone loss caused by hindlimb suspension and improves the bone strength in the proximal and distal femur. We employed the hindlimb suspension model, which simulates conditions like bed rest, making it suitable for our study. This model is widely recognized for characterizing disuse-induced bone and muscle loss [13], as it eliminates or reduces ground reaction force while maintaining muscle contraction [2]. In this study, the body weight of HS rats was significantly lower than that of the controls, consistent with previous findings [19,20]. However, transcutaneous CO_2 application did not significantly alter weight loss, even after hindlimb suspension. Our previous phase I clinical study on the topical cutaneous application of CO_2 for fracture repair showed that CO_2 therapy is safe for humans with no adverse events [21]. The current results regarding body weight further support treatment safety.

Moreover, hindlimb suspension led to gastrocnemius muscle atrophy, as evidenced by changes in muscle weight and myofiber CSA. Genetic analysis revealed decreased IGF-1 expression and increased Atrogin-1 in unloaded muscles. These findings align with previous studies, which have shown that hindlimb suspension induces muscle atrophy at unloaded sites [22]. In atrophying muscles, the IGF-phosphoinositide 3-kinase (PI3K)-AKT pathway is suppressed, and Atrogin-1 expression is remarkably increased [23]. Similarly, IGF-1 expression in unloaded muscle decreases, and the PI3K-AKT pathway is also suppressed [24]. PGC-1α, which is induced in skeletal muscle by exercise, is known to suppress muscle atrophy [25]. In muscles, PGC-1α mediates responses such as mitochondrial biogenesis, muscle fiber-type switching, VEGF upregulation, and neovascularization [26]. Hindlimb suspension reduces PGC-1α expression in the soleus but not in the gastrocnemius or plantaris [27–29]. Our results showed no significant difference in PGC-1α expression between unloaded and control rats in the gastrocnemius. Given that fast muscles primarily rely on glycolytic metabolism and have low PGC-1α expression [30], we predict that hindlimb suspension impacts PGC-1α expression more in slow muscles like the soleus than in fast muscles like the gastrocnemius.

In contrast, transcutaneous CO_2 application mitigated muscle atrophy by upregulating VEGF and PGC-1α. Our previous study showed that CO_2 application induced PGC-1α expression in the rat tibialis anterior muscle, mediating exercise-related responses [8]. Similarly, CO_2 therapy enhanced muscle oxidative capacity via eNOS and PGC-1α signaling in a type 1 diabetes rat model [31]. Our findings align with these studies, showing suppressed mRNA expression of MuRF1 and Atrogin-1 and elevated IGF-1 expression in the gastrocnemius of CO_2-treated rats.

In the treated group, capillary densities surrounding the muscle fibers increased, along with the activation of angiogenesis and blood flow markers VEGF and eNOS. In a previous study, transgenic mice overexpressing PGC-1 exhibited smaller reductions in muscle fiber diameter and lower induction of Atrogin-1 and MuRF-1 after denervation and fasting compared to controls [25]. The PGC-1α4 isoform specifically induces IGF-1, leading to myotube hypertrophy [32]. Activation of PGC-1α and IGF-1 likely increases the expression of angiogenesis markers [25,32]. Therefore, PGC-1α plays a crucial role in the preventive mechanism of transcutaneous CO_2 application for disuse muscle

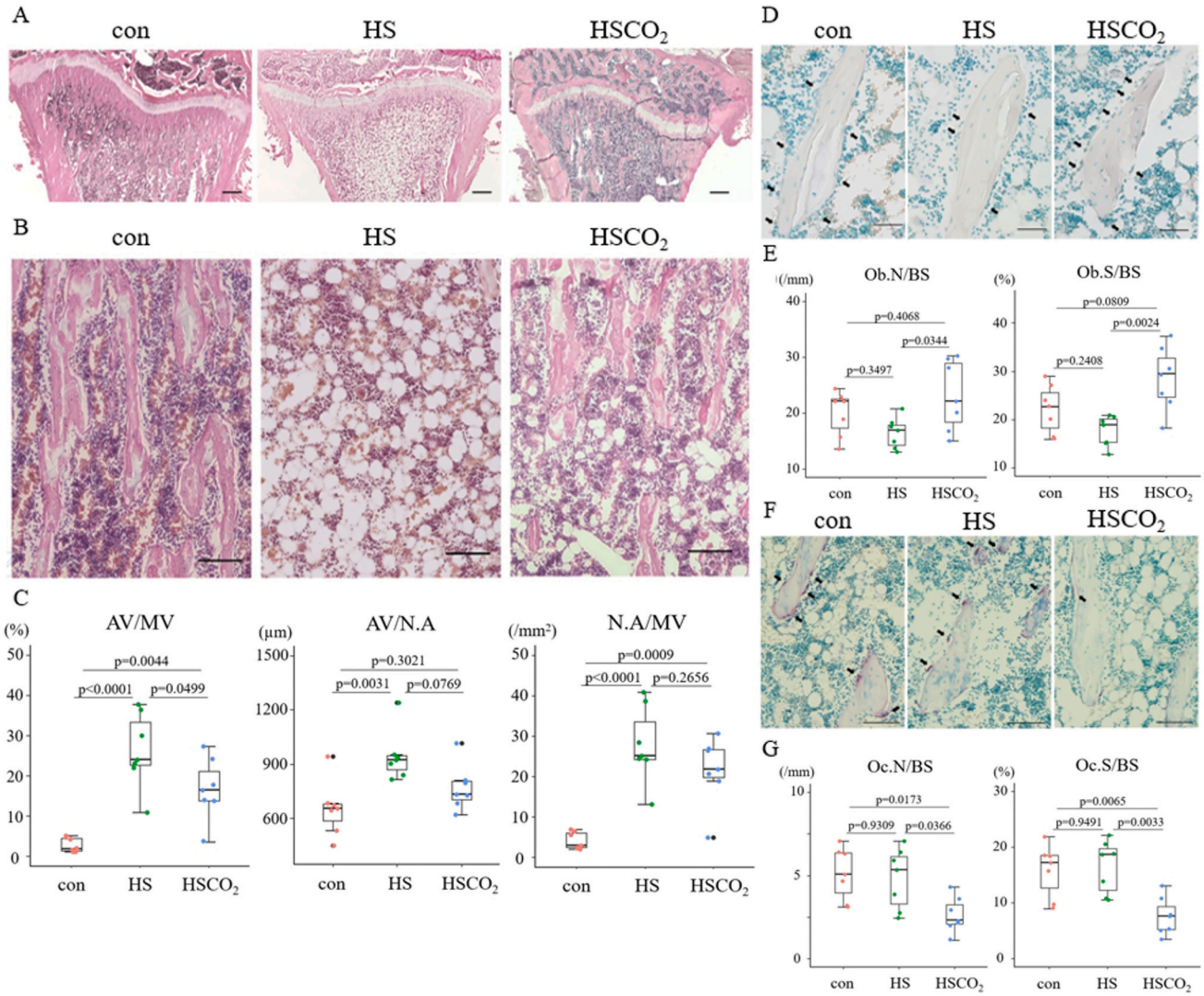

Fig. 4. Histological assessments of the proximal metaphyseal tibia. (A, B) Representative H&E staining in the proximal metaphyseal tibia from the control, HS, and $HSCO_2$ rats. HS rats exhibited more adipose tissue than control rats, whereas less $HSCO_2$ rats showed a lower amount than HS rats. A: Magnification ×40. Scale bar, 500 μm, B: Magnification ×200. Scale bar, 100 μm. (C) Quantitative analysis of AV/MV, AV/N.A, and N.A/MV in the proximal metaphyseal tibia based on H&E images. (D) Representative ALP staining of the proximal metaphyseal tibia from the control, HS, and $HSCO_2$ rats. Scale bar, 50 μm. Arrowheads point to osteoblasts on the surface of trabecular bone in each image. (E) Quantitative measurements of Ob.S/BS and Ob.N/BS in the proximal metaphyseal tibia measured based on ALP staining images. (F) Representative TRAP staining in the proximal metaphyseal tibia from the control, HS, and $HSCO_2$ rats. Scale bar, 100 μm. Arrowheads point to osteoclasts on the surface of trabecular bone in each image. (G) Quantitative measurements of Oc.S/BS and Oc.N/BS in the proximal metaphyseal tibia based on TRAP staining images. Data are presented as box plots with an indication of the median; whiskers represent minimum to maximum values and show all points, n = 7. Outlier data points are indicated with a black dot beside them. Comparisons were performed using one-way ANOVA followed by Tukey's test. All the quantification analyses were performed using the ImageJ software.

atrophy.

In our previous research, we investigated the effect of transcutaneous CO_2 application on the tibialis anterior muscle by comparing a CO_2-treatedand group with a grand control group that did not receive CO_2 treatment [8]. The findings from that study revealed both protein and gene upregulation of VEGF and PGC-1α in the CO_2-treated rats, although there was no significant difference in muscle weight, similar to our current findings. These combined results suggest that the effects of transcutaneous CO_2 application are not limited to disuse muscle atrophy but may also extend to normal muscle conditions.

In previous studies using hindlimb suspension rodent models, both cortical and trabecular bone mass and osteoblast activity decreased [13], whereas marrow adipose tissue increased [33]. In the present study, μCT analysis also showed significant reductions in cortical and trabecular parameters in the hindlimb suspension rats. Although the biomechanical assessment revealed no difference from control rats in the three-point bending test, there was significant weakness in compression tests. Bone loss caused by unloading is greater in the metaphysis than in the diaphysis, although both are affected [34], which may explain the biomechanical findings from our study. The reduction in proximal tibia marrow adipose tissue following hindlimb suspension aligns with the results of prior research [35]. Although osteoblast activity trended downward post-suspension, the change was not statistically significant. Hindlimb suspension leads to decreased osteogenic potential and increased adipogenic potential in femur-derived stem cells [36], suggesting a shift towards adipogenic differentiation, contributing to bone atrophy. The increased accumulation of marrow adipose tissue occurs at the expense of bone formation, which impairs osteogenic regeneration and hematopoiesis [37]. This is clinically correlated with osteoporosis and an elevated risk of fractures [38]. These studies suggest that inhibiting the accumulation of marrow adipose tissue could be a potential therapeutic strategy for treating osteoporosis. The regulation

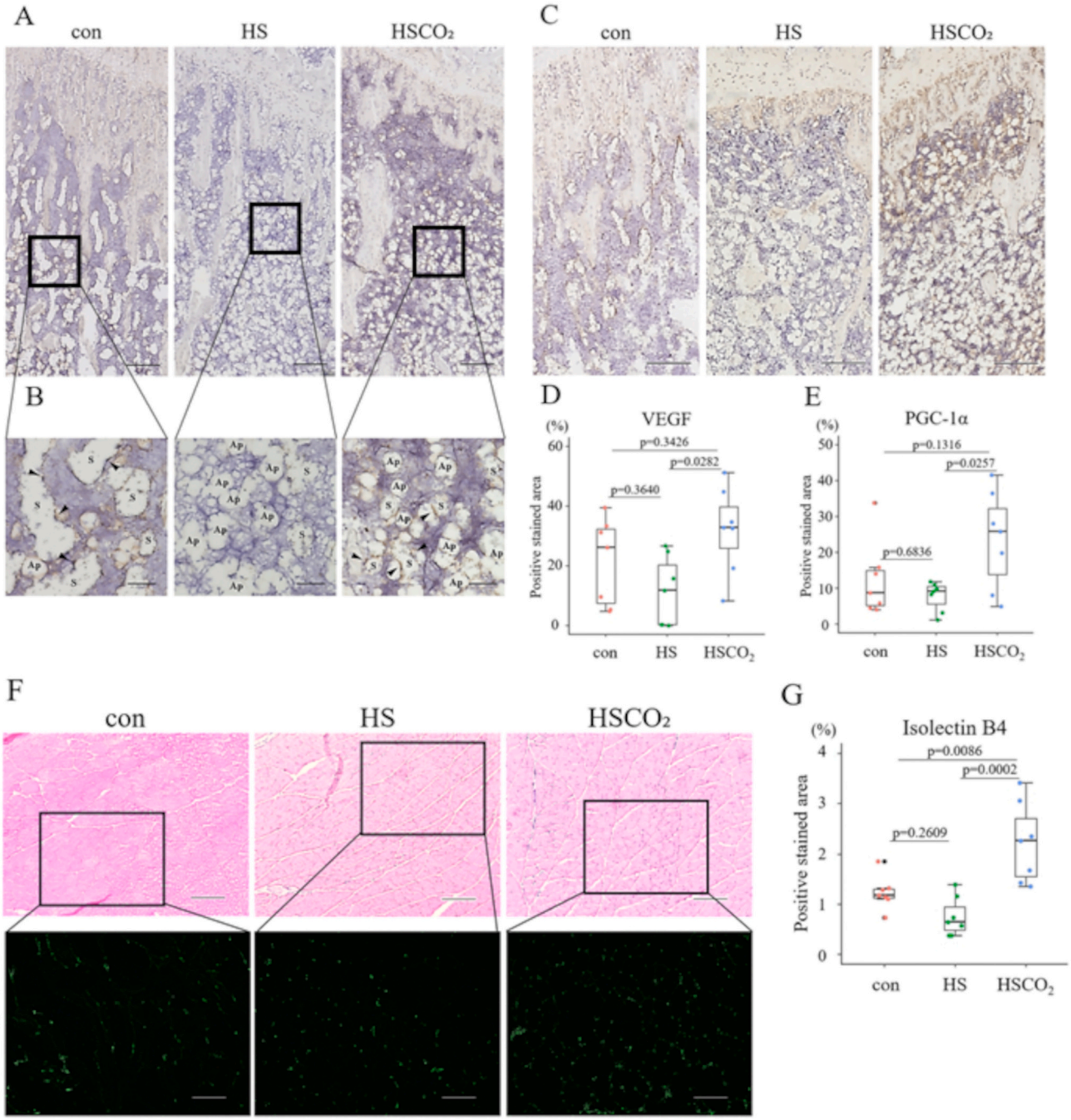

Fig. 5. Immunohistochemical assessments of the proximal metaphyseal tibia and gastrocnemius. (A, B) Representative IHC of VEGF in the proximal metaphyseal tibia from the control, HS, and $HSCO_2$ rats. A: Scale bar 200 μm. B: In the control rats, there are a few adipocytes and many large sinusoids. VEGF-positive endothelial cells are observed within the wall of sinusoids. In the HS rats, there are more adipocytes and fewer sinusoids VEGF-positive endothelial cells than the control rats. In the $HSCO_2$ rats, more VEGF-positive endothelial cells and sinusoids are observed than in the HS rats. Ap: adipocyte, S: sinusoid, Arrow head: Stained endothelial cell. Scale bar 50 μm. (C) Representative IHC of PGC-1α in the proximal metaphyseal tibia from the control, HS, and $HSCO_2$ rats. Scale bar 200 μm. (D) Quantification analysis of positive stained area of VEGF. (E) Quantification analysis of the positively stained area of PGC-1α. (F) Representative images of H&E staining and fluorescent detection in IHC of isolectin B4 in the gastrocnemius from the control, HS, and $HSCO_2$ rats. H&E staining: Scale bar 200 μm. IHC of isolectin B4: Scale bar 200 μm. (G) Quantification analysis of positive stained area of isolectin B4. Data are presented as box plots with the indication of the median; whiskers represent minimum to maximum values and show all points, n = 7. Outlier data points are indicated with a black dot beside them. Comparisons were performed using one-way ANOVA followed by Tukey's test. All the quantification analyses were performed using the ImageJ software.

of bone-fat balance by PGC-1α via skeletal stem cell lineage decisions has been investigated [39]. We hypothesized that the accumulation of marrow adipose tissue could be related to the downregulation of PGC-1α. However, PGC-1α expression was not significantly inhibited in the unloaded bones. To date, no studies have documented the suppression of PGC-1α expression in unloaded bones. Therefore, further investigation is warranted to elucidate the impact of mechanical loading on PGC-1α expression and marrow adipose tissue accumulation in bones.

Transcutaneous CO_2 application counteracted bone atrophy by significantly increasing VEGF and PGC-1α expression. To our knowledge, this study is the first to demonstrate the preventative potential of transcutaneous CO_2 therapy against disuse osteoporosis. CO_2 therapy

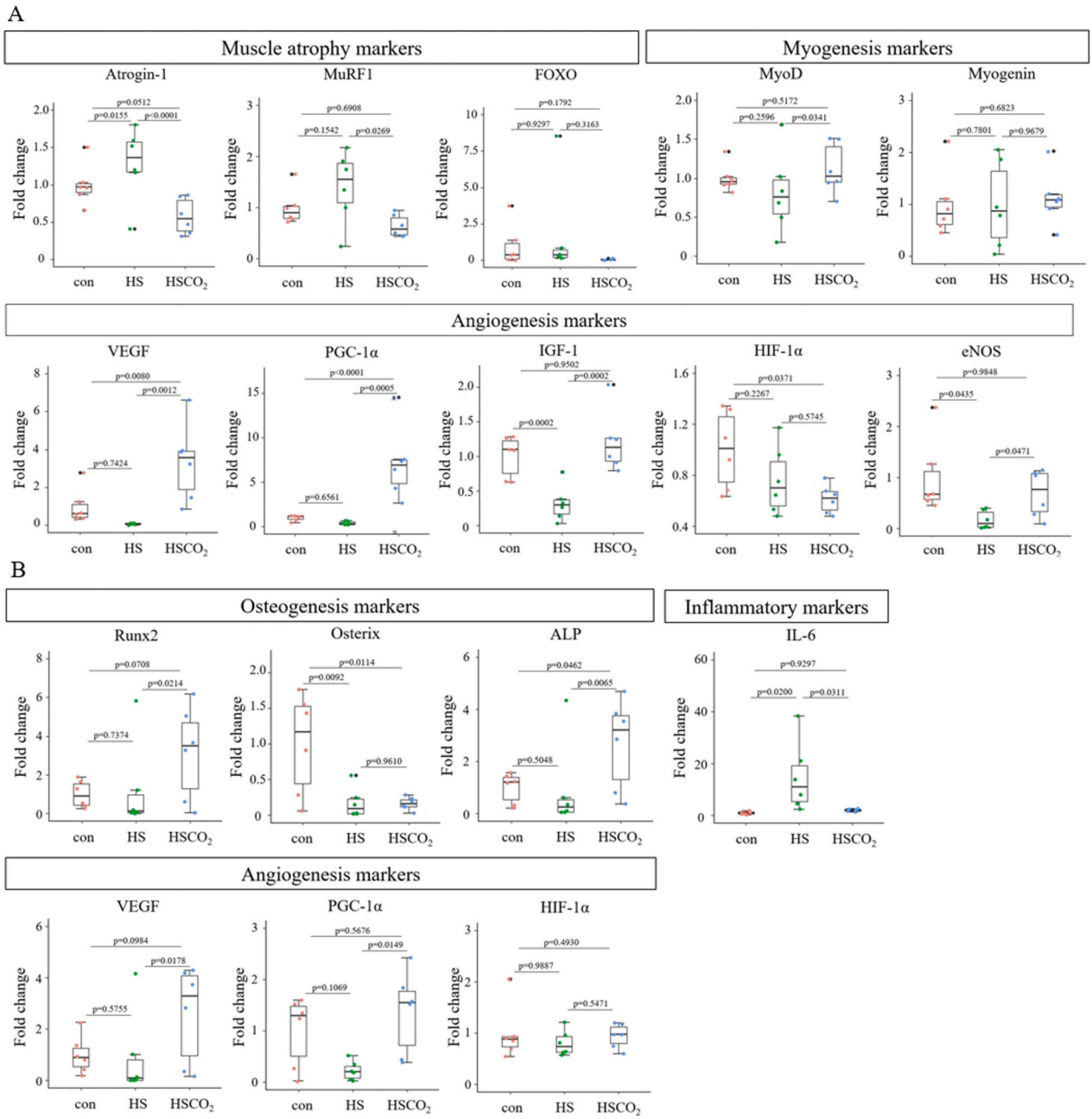

Fig. 6. Gene expression in bones and muscles evaluated with real-time RT-PCR. (A) Myogenesis, muscle atrophy, and angiogenesis markers in the gastrocnemius were analyzed. (B) Osteogenesis, inflammatory, osteoclast, and angiogenesis markers in the femur were analyzed. Gene expression levels were normalized to those of *GAPDH* and are presented as fold change relative to a sample of the control group. Data are presented as box plots with the indication of the median; whiskers represent minimum to maximum values and show all points, $n = 6$. Outlier data points are indicated with a black dot beside them. Comparisons were performed using one-way ANOVA followed by Tukey's test.

promoted osteoblast activity while inhibiting marrow adipogenesis, which contrasts with the effects of hindlimb suspension and is consistent with the role of PGC-1α. Marrow adipose tissue compresses the sinus wall, reducing the sinus caliber [18]. IHC analysis revealed that VEGF-positive endothelial cells in the sinusoids wall were prominent in rats that underwent CO_2 therapy. This suggests that the reduction of bone marrow adipose tissue accumulation due to CO_2 therapy promoted increased angiogenesis in the bone marrow. Our previous study, using laser Doppler to assess blood flow immediately after CO_2 therapy on fractured rat limbs, revealed that this treatment increased blood flow not only at the fracture site but throughout the entire limb [5]. This supports our current hypothesis and suggests that the effect of this treatment may extend beyond disuse induced by hindlimb suspension. Genetic analysis of the distal femur revealed elevated expression of Runx2, ALP, and VEGF, indicating enhanced angiogenesis and osteogenesis, likely owing to molecular crosstalk between endothelial and osteoblastic cells [40]. These findings suggest that CO_2 therapy may mitigate disuse osteoporosis, implicating PGC-1α in its mechanism.

Here, osteoclast activity assessed by TRAP staining in HS rats was similar to that in control rats. In previous experimental studies using rodent models of hindlimb unloading, both increased and lack of increased osteoclast activity have been reported [41,42]. One study found that hindlimb-unloaded animals that lost weight or failed to gain weight showed elevated osteoclast activity, although this response was transient [42]. This increase may be attributed to systemic stress [13]. Osteoclasts are affected by mechanical stress similar to osteoblasts and

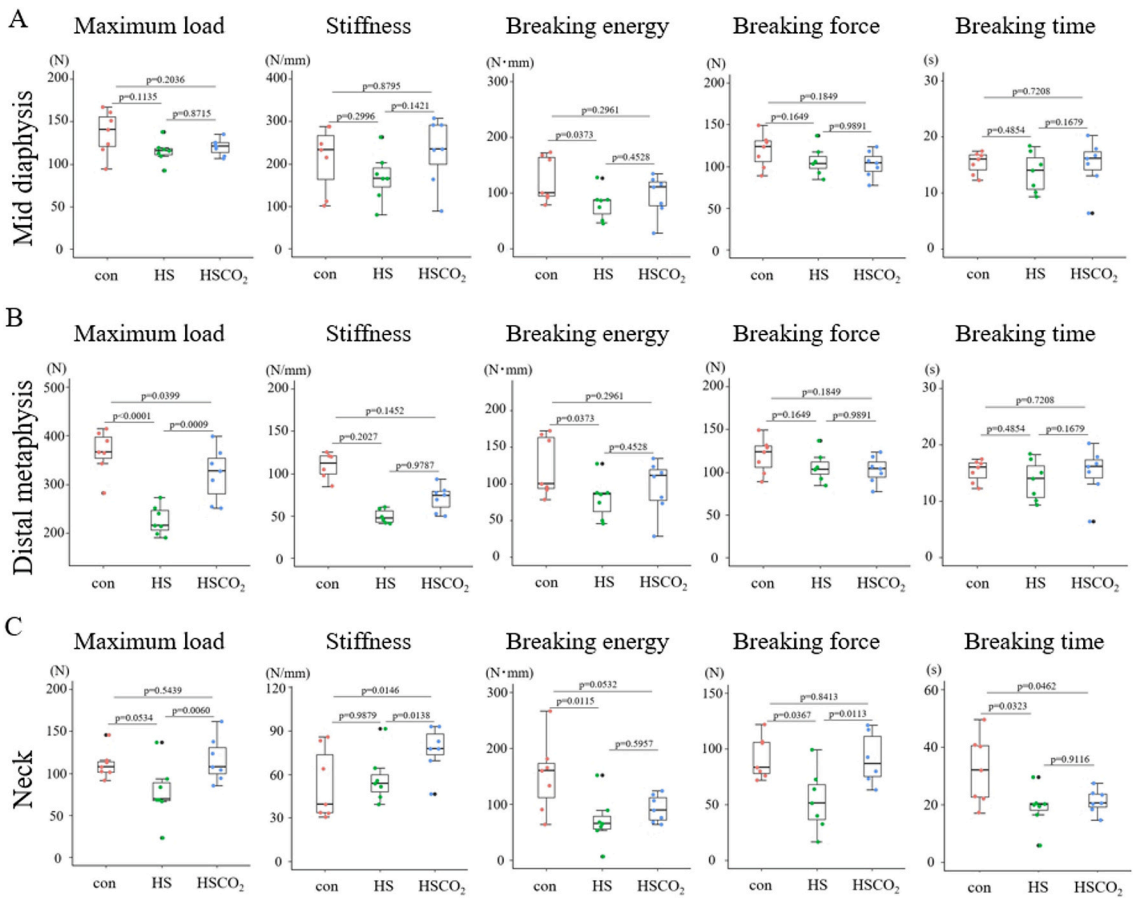

Fig. 7. Biomechanical assessments of the femurs. (A) The three-point bend test was performed to analyze the strength of the femoral mid-diaphysis. (B) The compression test of the distal femoral metaphysis. (C) The compression test of the femoral neck. Maximum load, stiffness, breaking energy, breaking force, and breaking time were assessed in each test. Data are presented as box plots with the indication of the median; whiskers represent minimum to maximum values and show all points, n = 7. Outlier data points are indicated with a black dot beside them. Comparisons were performed using one-way ANOVA followed by Tukey's test.

osteocytes [43]. After, 3 weeks of hindlimb suspension, an increase in the osteoclast surface and inflammatory cytokines in osteocytes in rats was observed [19]. Hence, inflammatory cytokines influence osteoclast activity due to hindlimb suspension. The upregulated IL-6 expression in the distal femur of hindlimb-suspended rats may be linked to the relationship between inflammation and osteoclast activity.

Here, transcutaneous CO_2 application suppressed the number and activity of osteoclasts and IL-6 expression. We hypothesized that the anti-inflammatory effect of CO_2 may be involved in the suppression of osteoclasts. Proinflammatory factors such as IL-6 and TNF-α increase osteoclast activity via both RANKL and RANK-independent pathways [44,45]. CO_2 exerts an anti-inflammatory effect by binding to ubiquitin. After binding, it undergoes remodeling and transforms into a proteasome that directly diminishes the NF-kB response [46]. CO_2 treatment promoted ERK1/2 activity but mitigated overactivated ERK1/2, exerting anti-inflammatory effects on human umbilical vein endothelial cells [47]. Moreover, our previous study showed that transcutaneous CO_2 application significantly reduced both osteoclast and inflammatory activity in metastatic bone tumors [7]. The suppression of osteoclast activity by CO_2 therapy may also be influenced by increased PGC-1α expression. PGC-1α suppresses inflammation in muscle cells by modulating the NF-kB pathway [48]. Loss of PGC-1α in bone marrow mesenchymal cells could increase NF-kB-dependent expression of proinflammatory cytokines, thereby enhancing osteoclast activation [39]. These previous findings support our hypothesis that the anti-inflammatory effect of CO_2, coupled with PGC-1α upregulation, contributes to the suppression of osteoclast activity and bone resorption.

This study has several limitations. First, the molecular mechanism underlying the increase in PGC-1α expression in the muscle and bone caused by CO_2 therapy, remains unclear. PGC-1α is activated by exercise via calcium-dependent protein phosphatase calcineurin and calmodulin-dependent kinase signals [49]. Whether a similar mechanism is involved in CO_2 therapy is unknown. Further investigation, including the use of knockout mice of PGC-1α, is needed to elucidate this mechanism. Second, we did not consider the bone-muscle interactions affected by CO_2 therapy. Muscle and bone atrophic changes caused by hindlimb suspension are related to muscle myokines [20]. To assess this, myokine expression at multiple time points must be considered.

In conclusion, transcutaneous CO_2 application presents a promising novel approach for preventing disuse osteoporosis and muscle atrophy by promoting local angiogenesis. PGC-1α plays a crucial role in facilitating this angiogenic pathway. Transcutaneous CO_2 application is a low-cost, non-invasive treatment that requires only CO_2 and a hydrogel, making it easy to apply to specific local site. Further studies, including investigations on the underlying mechanism and clinical trials, is needed to explore the full potential and indications of this treatment.

Funding

This research did not receive any specific grant from funding agencies in the public, commercial, or not-for-profit sectors.

CRediT authorship contribution statement

Ryota Nishida: Writing – original draft, Visualization, Investigation, Formal analysis. **Tomoaki Fukui:** Writing – review & editing, Funding

acquisition, Conceptualization. **Takahiro Niikura:** Conceptualization. **Yohei Kumabe:** Validation. **Ryo Yoshikawa:** Methodology. **Kyohei Takase:** Validation. **Yuya Yamamoto:** Validation. **Ryosuke Kuroda:** Supervision. **Keisuke Oe:** Project administration.

Declaration of competing interest

The authors declare that they have no known competing financial interests or personal relationships that could have appeared to influence the work reported in this paper.

Data availability

Data will be made available on request.

Acknowledgments

We extend our sincere gratitude to Ms. Kyoko Tanaka, Maya Yasuda, Minako Nagata, and Jonathan (Department of Orthopaedic Surgery, Kobe University Graduate School of Medicine, Kobe, Japan) for their technical assistance throughout this study.

Appendix A. Supplementary data

Supplementary data to this article can be found online at https://doi.org/10.1016/j.bone.2024.117262.

References

[1] US Department of Health and Human Services, Bone Health and Osteoporosis: A Report of the Surgeon General, United States Department of Health and Human Services, Office of the Surgeon General, Rockville, Maryland, 2004.
[2] T. Bettis, B.J. Kim, M.W. Hamrick, Impact of muscle atrophy on bone metabolism and bone strength: implications for muscle-bone crosstalk with aging and disuse, Osteoporos. Int. 29 (2018) 1713–1720, https://doi.org/10.1007/s00198-018-4570-1.
[3] A.M. Nyholm, K. Gromov, H. Palm, M. Brix, T. Kallemose, A. Troelsen, Danish Fracture Database Collaborators, Time to surgery is associated with thirty-day and ninety-day mortality after proximal femoral fracture: a retrospective observational study on prospectively collected data from the Danish fracture database collaborators, J. Bone Joint Surg. Am. 97 (2015) 1333–1339, https://doi.org/10.2106/JBJS.O.00029.
[4] P.A. Gholve, K.P. Kosygan, S.W. Sturdee, A.A. Faraj, Multidisciplinary integrated care pathway for fractured neck of femur. A prospective trial with improved outcome, Injury 36 (2005) 93–98, https://doi.org/10.1016/j.injury.2004.02.007 (discussion 99).
[5] T. Koga, T. Niikura, S.Y. Lee, E. Okumachi, T. Ueha, T. Iwakura, Y. Sakai, M. Miwa, R. Kuroda, M. Kurosaka, Topical cutaneous CO_2 application by means of a novel hydrogel accelerates fracture repair in rats, J. Bone Joint Surg. Am. 96 (2014) 2077–2084, https://doi.org/10.2106/JBJS.M.01498.
[6] Y. Kuroiwa, T. Fukui, S. Takahara, S.Y. Lee, K. Oe, M. Arakura, Y. Kumabe, T. Oda, T. Matsumoto, T. Matsushita, T. Akisue, Y. Sakai, R. Kuroda, T. Niikura, Topical cutaneous application of CO_2 accelerates bone healing in a rat femoral defect model, BMC Musculoskelet. Disord. 20 (2019) 237, https://doi.org/10.1186/s12891-019-2601-5.
[7] T. Takemori, T. Kawamoto, T. Ueha, M. Toda, M. Morishita, E. Kamata, N. Fukase, H. Hara, S. Fujiwara, T. Niikura, R. Kuroda, T. Akisue, Transcutaneous carbon dioxide application suppresses bone destruction caused by breast cancer metastasis, Oncol. Rep. 40 (2018) 2079–2087, https://doi.org/10.3892/or.2018.6608.
[8] K. Oe, T. Ueha, Y. Sakai, T. Niikura, S.Y. Lee, A. Koh, T. Hasegawa, M. Tanaka, M. Miwa, M. Kurosaka, The effect of transcutaneous application of carbon dioxide (CO_2) on skeletal muscle, Biochem. Biophys. Res. Commun. 407 (2011) 148–152, https://doi.org/10.1016/j.bbrc.2011.02.128.
[9] H. Nishimoto, A. Inui, T. Ueha, M. Inoue, S. Akahane, R. Harada, Y. Mifune, T. Kokubu, K. Nishida, R. Kuroda, Y. Sakai, Transcutaneous carbon dioxide application with hydrogel prevents muscle atrophy in a rat sciatic nerve crush model, J. Orthop. Res. 36 (2018) 1653–1658, https://doi.org/10.1002/jor.23817.
[10] M. Inoue, Y. Sakai, K. Oe, T. Ueha, T. Koga, H. Nishimoto, S. Akahane, R. Harada, S.Y. Lee, T. Niikura, R. Kuroda, Transcutaneous carbon dioxide application inhibits muscle atrophy after fracture in rats, J. Orthop. Sci. 25 (2020) 338–343, https://doi.org/10.1016/j.jos.2019.03.024.
[11] Y. Sakai, M. Miwa, K. Oe, T. Ueha, A. Koh, T. Niikura, T. Iwakura, S.Y. Lee, M. Tanaka, M. Kurosaka, A novel system for transcutaneous application of carbon dioxide causing an "artificial Bohr effect" in the human body, PLoS One 6 (2011) e24137, https://doi.org/10.1371/journal.pone.0024137.
[12] A.P. Kusumbe, S.K. Ramasamy, R.H. Adams, Coupling of angiogenesis and osteogenesis by a specific vessel subtype in bone, Nature 507 (2014) 323–328, https://doi.org/10.1038/nature13145.
[13] E.R. Morey-Holton, R.K. Globus, Hindlimb unloading of growing rats: a model for predicting skeletal changes during space flight, Bone 22 (5) (1998) 83S–88S, https://doi.org/10.1016/s8756-3282(98)00019-2 (Suppl).
[14] E.R. Morey-Holton, R.K. Globus, Hindlimb unloading rodent model: technical aspects, J. Appl. Physiol. 92 (2002) (1985) 1367–1377, https://doi.org/10.1152/japplphysiol.00969.2001.
[15] Y. Gabet, D. Kohavi, R. Müller, M. Chorev, I. Bab, Intermittently administered parathyroid hormone 1–34 reverses bone loss and structural impairment in orchiectomized adult rats, Osteoporos. Int. 16 (2005) 1436–1443, https://doi.org/10.1007/s00198-005-1876-6.
[16] K. Nozaka, N. Miyakoshi, Y. Kasukawa, S. Maekawa, H. Noguchi, Y. Shimada, Intermittent administration of human parathyroid hormone enhances bone formation and union at the site of cancellous bone osteotomy in normal and ovariectomized rats, Bone 42 (2008) 90–97, https://doi.org/10.1016/j.bone.2007.08.041.
[17] L. Tornvig, L.I. Mosekilde, J. Justesen, E. Falk, M. Kassem, Troglitazone treatment increases bone marrow adipose tissue volume but does not affect trabecular bone volume in mice, Calcif. Tissue Int. 69 (2001) 46–50, https://doi.org/10.1007/s002230020018.
[18] P. Bianco, Bone and the hematopoietic niche: a tale of two stem cells, Blood 117 (2011) 5281–5288, https://doi.org/10.1182/blood-2011-01-315069.
[19] C.E. Metzger, S. Anand Narayanan, P.H. Phan, S.A. Bloomfield, Hindlimb unloading causes regional loading-dependent changes in osteocyte inflammatory cytokines that are modulated by exogenous irisin treatment, npj Microgravity 6 (2020) 28, https://doi.org/10.1038/s41526-020-00118-4.
[20] G. Colaianni, T. Mongelli, C. Cuscito, P. Pignataro, L. Lippo, G. Spiro, A. Notarnicola, I. Severi, G. Passeri, G. Mori, G. Brunetti, B. Moretti, U. Tarantino, S.C. Colucci, J.E. Reseland, R. Vettor, S. Cinti, M. Grano, Irisin prevents and restores bone loss and muscle atrophy in hind-limb suspended mice, Sci. Rep. 7 (2017) 2811, https://doi.org/10.1038/s41598-017-02557-8.
[21] T. Niikura, T. Iwakura, T. Omori, S.Y. Lee, Y. Sakai, T. Akisue, K. Oe, T. Fukui, T. Matsushita, T. Matsumoto, R. Kuroda, Topical cutaneous application of carbon dioxide via a hydrogel for improved fracture repair: results of phase I clinical safety trial, BMC Musculoskelet. Disord. 20 (2019) 563, https://doi.org/10.1186/s12891-019-2911-7.
[22] D.B. Thomason, F.W. Booth, Atrophy of the soleus muscle by hindlimb unweighting, J. Appl. Physiol. 68 (1990) (1985) 1–12, https://doi.org/10.1152/jappl.1990.68.1.1.
[23] M. Sandri, C. Sandri, A. Gilbert, C. Skurk, E. Calabria, A. Picard, K. Walsh, S. Schiaffino, S.H. Lecker, A.L. Goldberg, Foxo transcription factors induce the atrophy-related ubiquitin ligase Atrogin-1 and cause skeletal muscle atrophy, Cell 117 (2004) 399–412, https://doi.org/10.1016/s0092-8674(04)00400-3.
[24] B. Han, M.J. Zhu, C. Ma, M. Du, Rat hindlimb unloading down-regulates insulin like growth factor-1 signaling and AMP-activated protein kinase, and leads to severe atrophy of the soleus muscle, Appl. Physiol. Nutr. Metab. 32 (2007) 1115–1123, https://doi.org/10.1139/H07-102.
[25] M. Sandri, J. Lin, C. Handschin, W. Yang, Z.P. Arany, S.H. Lecker, A.L. Goldberg, B. M. Spiegelman, PGC-1alpha protects skeletal muscle from atrophy by suppressing FoxO3 action and atrophy-specific gene transcription, Proc. Natl. Acad. Sci. USA 103 (2006) 16260–16265, https://doi.org/10.1073/pnas.0607795103.
[26] Z. Arany, S.Y. Foo, Y. Ma, J.L. Ruas, A. Bommi-Reddy, G. Girnun, M. Cooper, D. Laznik, J. Chinsomboon, S.M. Rangwala, K.H. Baek, A. Rosenzweig, B. M. Spiegelman, HIF-independent regulation of VEGF and angiogenesis by the transcriptional coactivator PGC-1α, Nature 451 (2008) 1008–1012, https://doi.org/10.1038/nature06613.
[27] J. Cannavino, L. Brocca, M. Sandri, R. Bottinelli, M.A. Pellegrino, PGC1-α over-expression prevents metabolic alterations and soleus muscle atrophy in hindlimb unloaded mice, J. Physiol. 592 (2014) 4575–4589, https://doi.org/10.1113/jphysiol.2014.275545.
[28] F. Nagatomo, H. Fujino, H. Kondo, H. Suzuki, M. Kouzaki, I. Takeda, A. Ishihara, PGC-1α and FOXO1 mRNA levels and fiber characteristics of the soleus and plantaris muscles in rats after hindlimb unloading, Histol. Histopathol. 26 (2011) 1545–1553, https://doi.org/10.14670/HH-26.1545.
[29] J. Cannavino, L. Brocca, M. Sandri, B. Grassi, R. Bottinelli, M.A. Pellegrino, The role of alterations in mitochondrial dynamics and PGC-1α over-expression in fast muscle atrophy following hindlimb unloading, J. Physiol. 593 (2015) 1981–1995, https://doi.org/10.1113/jphysiol.2014.286740.
[30] J. Lin, H. Wu, P.T. Tarr, C.Y. Zhang, Z. Wu, O. Boss, L.F. Michael, P. Puigserver, E. Isotani, E.N. Olson, B.B. Lowell, R. Bassel-Duby, B.M. Spiegelman, Transcriptional co-activator PGC-1α drives the formation of slow-twitch muscle fibres, Nature 418 (2002) 797–801, https://doi.org/10.1038/nature00904.
[31] T. Matsumoto, M. Tanaka, R. Nakanish, M. Takuwa, T. Hirabayashi, K. Ono, T. Ikeji, N. Maeshige, Y. Sakai, T. Akisue, H. Kondo, A. Ishihara, H. Fujino, Transcutaneous carbon dioxide attenuates impaired oxidative capacity in skeletal muscle in hyperglycemia model, Gen. Physiol. Biophys. 38 (2019) 237–244, https://doi.org/10.4149/gpb_2018048.
[32] J.L. Ruas, J.P. White, R.R. Rao, S. Kleiner, K.T. Brannan, B.C. Harrison, N. P. Greene, J. Wu, J.L. Estall, B.A. Irving, I.R. Lanza, K.A. Rasbach, M. Okutsu, K. S. Nair, Z. Yan, L.A. Leinwand, B.M. Spiegelman, A PGC-1α isoform induced by resistance training regulates skeletal muscle hypertrophy, Cell 151 (2012) 1319–1331, https://doi.org/10.1016/j.cell.2012.10.050.
[33] S. Ahdjoudj, F. Lasmoles, X. Holy, E. Zerath, P.J. Marie, Transforming growth factor β2 inhibits adipocyte differentiation induced by skeletal unloading in rat

bone marrow stroma, J. Bone Miner. Res. 17 (2002) 668–677, https://doi.org/10.1359/jbmr.2002.17.4.668.

[34] R.K. Globus, D.D. Bikle, E.R. Morey-Holton, The temporal response of bone to unloading, Endocrinology 118 (1986) 733–742, https://doi.org/10.1210/endo-118-2-733.

[35] C.N. Booker, C.L. Haga, S.V. Boregowda, J. Strivelli, D.G. Phinney, Transcriptional responses of skeletal stem/progenitor cells to hindlimb unloading and recovery correlate with localized but not systemic multi-systems impacts, npj Microgravity. 7 (2021) 49, https://doi.org/10.1038/s41526-021-00178-0.

[36] Z. Pan, J. Yang, C. Guo, D. Shi, D. Shen, Q. Zheng, R. Chen, Y. Xu, Y. Xi, J. Wang, Effects of hindlimb unloading on ex vivo growth and osteogenic/adipogenic potentials of bone marrow-derived mesenchymal stem cells in rats, Stem Cells Dev. 17 (2008) 795–804, https://doi.org/10.1089/scd.2007.0254.

[37] T.H. Ambrosi, A. Scialdone, A. Graja, S. Gohlke, A.M. Jank, C. Bocian, L. Woelk, H. Fan, D.W. Logan, A. Schürmann, L.R. Saraiva, T.J. Schulz, Adipocyte accumulation in the bone marrow during obesity and aging impairs stem cell-based hematopoietic and bone regeneration, Cell Stem Cell 20 (2017) 771–784.e6, https://doi.org/10.1016/j.stem.2017.02.009.

[38] P.K. Fazeli, M.C. Horowitz, O.A. MacDougald, E.L. Scheller, M.S. Rodeheffer, C. J. Rosen, A. Klibanski, Marrow fat and bone-new perspectives, J. Clin. Endocrinol. Metab. 98 (2013) 935–945, https://doi.org/10.1210/jc.2012-3634.

[39] B. Yu, L. Huo, Y. Liu, P. Deng, J. Szymanski, J. Li, X. Luo, C. Hong, J. Lin, C. Y. Wang, PGC-1α controls skeletal stem cell fate and bone-fat balance in osteoporosis and skeletal aging by inducing TAZ, Cell Stem Cell 23 (2018) 615–623, https://doi.org/10.1016/j.stem.2018.09.001.

[40] S.K. Ramasamy, A.P. Kusumbe, L. Wang, R.H. Adams, Endothelial Notch activity promotes angiogenesis and osteogenesis in bone, Nature 507 (2014) 376–380, https://doi.org/10.1038/nature13146.

[41] M.C. van der Meulen, E.R. Morey-Holton, D.R. Carter, Hindlimb suspension diminishes femoral cross-sectional growth in the rat, J. Orthop. Res. 13 (1995) 700–707, https://doi.org/10.1002/jor.1100130509.

[42] L. Vico, V.E. Novikov, J.M. Very, C. Alexandre, Bone histomorphometric comparison of rat tibial metaphysis after 7-day tail suspension vs. 7-day spaceflight, Aviat. Space Environ. Med. 62 (1991) 26–31.

[43] W. Sun, Y. Li, J. Li, Y. Tan, X. Yuan, H. Meng, J. Ye, G. Zhong, X. Jin, Z. Liu, R. Du, W. Xing, D. Zhao, J. Song, Y. Li, J. Pan, Y. Zhao, Q. Li, A. Wang, S. Ling, R. Dai, Y. Li, Mechanical stimulation controls osteoclast function through the regulation of Ca^{2+}-activated Cl^{-} channel Anoctamin 1, Commun. Biol. 6 (2023) 407, https://doi.org/10.1038/s42003-023-04806-1.

[44] W. O'Brien, B.M. Fissel, Y. Maeda, J. Yan, X. Ge, E.M. Gravallese, A.O. Aliprantis, J. F. Charles, RANK-independent osteoclast formation and bone erosion in inflammatory arthritis, Arthritis Rheum. 68 (2016) 2889–2900, https://doi.org/10.1002/art.39837.

[45] M.S. Nanes, Tumor necrosis factor-α: molecular and cellular mechanisms in skeletal pathology, Gene 321 (2003) 1–15, https://doi.org/10.1016/s0378-1119(03)00841-2.

[46] C.E. Keogh, C.C. Scholz, J. Rodriguez, A.C. Selfridge, A. Von Kriegsheim, E. P. Cummins, Carbon dioxide-dependent regulation of NF-κB family members RelB and p100 gives molecular insight into CO_2-dependent immune regulation, J. Biol. Chem. 292 (2017) 11561–11571, https://doi.org/10.1074/jbc.M116.755090.

[47] H. Galganska, W. Jarmuszkiewicz, L. Galganski, Carbon dioxide inhibits COVID-19-type proinflammatory responses through extracellular signal-regulated kinases 1 and 2, novel carbon dioxide sensors, Cell. Mol. Life Sci. 78 (2021) 8229–8242, https://doi.org/10.1007/s00018-021-04005-3.

[48] P.S. Eisele, S. Salatino, J. Sobek, M.O. Hottiger, C. Handschin, The peroxisome proliferator-activated receptor γ coactivator 1α/β (PGC-1) coactivators repress the transcriptional activity of NF-κB in skeletal muscle cells, J. Biol. Chem. 288 (2013) 2246–2260, https://doi.org/10.1074/jbc.M112.375253.

[49] C. Handschin, J. Rhee, J. Lin, P.T. Tarr, B.M. Spiegelman, An autoregulatory loop controls peroxisome proliferator-activated receptor gamma coactivator 1alpha expression in muscle, Proc. Natl. Acad. Sci. USA 100 (2003) 7111–7116, https://doi.org/10.1073/pnas.1232352100.